AIAA Journal, Available online 28 November 2017
DOI:10.2514/1.J056560

Delay of dynamic stall using pulsed air jet vortex generators

R.B. Green[1], S.A. Prince[2], Y. Wang[1], V. Khodagolian[3], and F.N. Coton*[1]

[1]Aerospace Sciences Division, University of Glasgow, UK

[2]School of Aerospace, Transport and Manufacturing, Cranfield University, UK

[3]Department of Mechanical Engineering and Aeronautics, City University, London, UK

*AIAA Fellow

Nomenclature

AJVG	air jet vortex generator
a	damping coefficient computed with angles in radians
C_m	moment coefficient about quarter chord, positive nose-up
C_n	normal force coefficient
C_p	pressure coefficient, $C_p = \frac{p-p_\infty}{q_\infty}$
C_w	work coefficient computed with angles in radians
C_μ	jet momentum coefficient for 100% duty cycle, $\frac{J}{q_\infty c}$
$C_{\mu D}$	pulsed jet momentum coefficient with duty cycle D, $\frac{JD}{q_\infty c}$
c	model chord length [m]
D	AJVG pulsed waveform duty cycle (from 0 to 1)
F^+	non-dimensional jet blowing frequency, $F^+ = \frac{f x_{TE}}{U_\infty}$
f	pulsed jet blowing frequency [Hz]
J	jet momentum, $J = \dot{m} U_j$ [$\mathrm{kg\,s^{-2}}$]
k	airfoil pitching reduced frequency, $k = \frac{\omega c}{2U_\infty}$
$\dot{m}$	jet mass flow rate per unit jet orifice length [$\mathrm{kg\,m^{-1}\,s^{-1}}$]
p	model surface pressure [Pa]
p_∞	free stream static pressure [Pa]
q_∞	free stream dynamic pressure [Pa]
t	time [s]
x	chordwise position [m]
x_{TE}	chordwise distance of AJVG array to trailing edge [m]
U_j	jet velocity [$\mathrm{m\,s^{-1}}$]
U_∞	wind tunnel speed [$\mathrm{m\,s^{-1}}$]

α angle of attack [deg] or [rad] as appropriate

$\bar{\alpha}$ mean angle of attack [deg] or [rad] as appropriate

$\hat{\alpha}$ pitching angle half-amplitude [deg] or [rad] as appropriate

$\Xi(t)$ non-dimensional damping as function of time, computed with angles in radians

ω model pitching frequency [radians per second]

I Introduction

The occurrence of dynamic stall is a limiting factor for the flight envelope of a conventional helicopter, owing to the extreme aerodynamic loads and moments that occur during the event, see for example [1]. This principally affects the rotor blade on the retreating part of the rotor azimuth, and when outboard compressibility effects on the advancing side of the rotor azimuth are considered also, aerodynamic design of airfoil sections and blades for rotorcraft applications is very challenging indeed (for example [2], [3]). Flow control concepts for rotorcraft have been proposed and investigated for many years now, and these include leading edge slats, higher harmonic control, phased flap actuation, and blowing (for example [4], [5], [6], [7], [8], [9]). Of interest in the present note is how blowing using air jets may be used to control dynamic stall. [8] report findings of pulsed (zero net mass flux) and continuous blowing for dynamic stall control on a NACA 0015, with the pulsed excitation seen to be particularly effective. It is noteworthy that the results indicated much lower jet blowing momentum coefficient for a pulsed jet. Pulsed blowing experiments were described by [10] at the higher test Mach number of 0.3, and the issue of higher power requirements for pulsed blowing was raised as an important issue. The jet exit orifice shapes in this paper did not appear to be optimised in any way, but the approach was used for investigation of control of shock induced stall at higher Mach number in addition to dynamic stall. Low Reynolds number dynamic stall control for large amplitude oscillations by continuous blowing was demonstrated in a water tunnel by [11], and very large blowing coefficients were used but positive cycle damping was achieved. One of their conclusions that appeared to be at odds with other studies was that pulsed blowing did not appear to deliver the performance improvements that had been successfully demonstrated elsewhere, although relatively few pulsed test cases were considered. In addition to rotorcraft aerodynamics applications, dynamic stall is important for wind turbine performance, and [12] describe dynamic stall control on tests of a NACA0018 at Reynolds number up to 0.5 million.

Adaptive blowing was used where the intention of the control of blade lift is important to relieve blade root bending moment.

There are various methods of injecting momentum into a flow by blowing. Air-jet vortex generators involve blowing a directed jet through a narrow orifice skewed at an angle to the oncoming flow and set to a pitch angle relative to the local surface, [13] and [14]. AJVGs generate a vortex to promote mixing analogous to vortex generator vanes fixed to a wing surface, but they have the advantage that they can be deactivated unlike fixed vanes. AJVGs have been shown to achieve the same delay in static stall angle at a lower momentum coefficient for a more conventionally arranged steady jet. In the context of this current paper [9] reported results of dynamic stall tests conducted on an airfoil fitted with AJVGs. Tests were performed on a RAE9645 section using continuous blowing through spanwise arrays of AJVGs, the principal finding being that the jet array closer to the leading edge at $x/c = 0.12$ was more effective than one at the more downstream $x/c = 0.6$ chord location. This study used large amplitude (10^o) airfoil pitching oscillations. A higher blowing coefficient weakened the dynamic stall vortex, and the dynamic stall appeared to be suppressed at sufficiently high C_μ. Given the promise showed by pulsed blowing in other studies and the potential advantages offered by AJVGs, the work of [9] was followed by an additional set of tests using AJVGs designed for pulsed blowing. This paper presents an analysis of the results of these tests, and pitching moment excursion and cycle damping coefficient are considered. It is shown that, while steady blowing AJVGs are effective in delaying dynamic stall to higher mean angle of attack during an oscillatory test, pulsed AJVGs delay dynamic stall even further and achieve the effect at lower jet blowing momentum coefficient.

II Experimental details

Tests were conducted in the University of Glasgow "Handley-Page" wind tunnel. This is a low-speed, closed-return tunnel with a 1.52m high $\times$ 2.13m wide working section. The operating speed for the tests described in this paper was $U_\infty = 30\text{ms}^{-1}$, and the turbulence level in the test area is 1%. The dynamic stall system and AJVG layout are as used by [9]. The baseline airfoil shape for the tests described in this paper was RAE 9645, which is a 12% thick section representative of modern helicopter main rotor blade sections, and the chord length was $c = 0.5$m. Elliptical shaped end plates were placed inboard of the ends of the model to provide quasi-2D test conditions over an effective test span of 1.1m. The

array of 20 AJVGs was along the 12% chord position, thus the length scale for the non-dimensional excitation frequency is $x_{TE} = 0.44$m. The spanwise spacing of the AJVGs was 45mm, and each AJVG orifice had an exit area of 18mm^2 with the jet pitched at an angle 30^o to the local tangent to the airfoil surface and skewed by 60^o relative to the free-stream direction to match those used by [15]. The internal AJVG actuator air ducting system consisted of the plenum pipe which fed all of the 20 jets and was pressure regulated. Each AJVG was fitted with a Synerjet brand pulsed air injector. The air jet, injector and plenum assembly was isolated from the model structure as much as possible with vibration dampening material in an effort to reduce the vibrational noise emitted from the injectors affecting the pressure sensors. Measurements of AJVG exit pressure were taken during calibration tests of a single, isolated device, and these determined that in the case of pulsed jets the pulsed jet momentum coefficient $C_{\mu D}$ was simply factored by the pulsed waveform duty cycle D. Jet momentum coefficient C_μ was determined by monitoring the plenum pressure and a calibration using an air flow meter with the jet running in steady mode. Plenum pressure was then measured during the experiments. Steady jet momentum coefficient setting was repeatable to ± 0.0001.

A chordwise array of 39 surface mounted Kulite pressure transducers was fitted around the mid-span of the model. These had a $\pm$ 2.5 psi (17kPa) range with non-linearity of 0.2%, and were capable of responding at a rate of up to 5kHz. Details of the data acquisition system are given by [9], but data were sampled 10kHz per channel simultaneously. Base upon data acquisition system performance and transducer characteristics the accuracy of pressure measurement at the test dynamic pressure was $\pm$5Pa equivalent to a pressure coefficient C_p of $\pm$ 0.01. .

Test Reynolds number for the air jet tests is Re=1 million. Data reported in this paper are with the model executing a sinusoidal pitching waveform $\alpha = \bar{\alpha} + \hat{\alpha} \sin \omega t$ at reduced frequency $k = 0.103$ with pitch half-amplitude $\hat{\alpha} = 8^o$.

III Results and discussion

Processed data files for the results presented in this paper are available on an open access basis from the url: https://doi.org/10.17862/cranfield.rd.5001947

A Data analysis

Normal force overshoot and pitching moment excursion during dynamic stall are important parameters to consider, and damping coefficient a summarises usefully the adverse effect of dynamic stall over a pitching cycle. This is given by [16] and [11] as

$a = \frac{-C_w}{\pi \hat{\alpha}^2}$,

where C_w is the work coefficient given by

$C_w = \oint C_m(\alpha) d\alpha$.

Analysis by [17] compute the time-resolved damping $\Xi(t)$ for a model waveform that is a pure sinusoid. For model motion of the form $\alpha = \bar{\alpha} + \hat{\alpha}\sin(\omega t)$ $\Xi(t)$ is then

$\Xi(t) = \frac{-1}{\hat{\alpha}}\left(\tilde{C}_m \sin(\omega t) + \tilde{C}_m \cos(\omega t)\right)$

where $\tilde{C}_m$ is the Hilbert Transform of the moment coefficient C_m. The average value of $\Xi(t)$ is the cycle damping a for the same data. It is well-known that a clockwise portion of a $C_m \sim \alpha$ loop is negatively damped, but using the time resolved damping $\Xi(t)$ permits a more detailed analysis of the damping as a function of time. Calculation of all damping coefficients and associated parameters is done with the angle expressed in radians.

B Effect of jet actuation on cycle damping, pitching moment excursion and dynamic stall in oscillatory test

Figure 1 shows cycle damping data as the mean angle changes for no blowing and steady and pulsed blowing, with a particular emphasis upon where cycle damping coefficients change from positive to negative and the appearance of the clockwise moment loop. With no blowing the damping becomes negative between $\bar{\alpha} = 10^o$ and 12^o, while for steady and pulsed blowing the ranges are $\bar{\alpha} = 12^o \sim 14^o$ and $14^o \sim 16^o$ respectively for the blowing coefficients shown. In the figure the blowing coefficient is higher for the steady jet case, so it is immediately clear that the pulsed blowing in this case is more effective at delaying the onset of negative damping to higher mean angle. The additional benefit of the blowing is that the pitching moment excursion is relieved, so even if the damping is negative the pitching moment load is reduced in magnitude compared to the baseline case. Figure 2 shows the effect of momentum coefficient for steady and pulsed blowing for the deep dynamic stall case with mean angle

of attack of 16°. Damping coefficient becomes more negative as momentum coefficient increases for steady blowing. For pulsed blowing an increase in C_μ results in less negative cycle damping, pitching moment excursion is less extreme, and there is eventually a return to positive damping at the highest C_μ tested.

AJVG blowing clearly affects the dynamic stall of the airfoil, and a more detailed examination is useful. Cases for mean angle $\bar{\alpha} = 16°$ will be discussed, with a pulsed blowing case that gives positive damping, and with negatively damped behaviour for the unactuated and steady blowing cases; see figure 2 and $C_{\mu D}$=0.0021 for the pulsed case and $C_{\mu D}$=0.0028 for the steady case. Normal force and moment coefficient cycles are shown in figures 3 and 4 respectively. The unactuated baseline data are shown on the plots together with data from static (non-pitching) runs. C_n for the steady blown case is barely different from the unactuated case on the upstroke and for the initial part of the downstroke, but the size of the hysteresis loop is smaller. The pulse blown case is quite different, with no sudden drop in C_n at high α, and a very small hysteresis loop indeed. C_m data for the same cases are shown in figure 4. The steady blown case is slightly negatively damped, and the shrinkage of the clockwise portion of the C_m cycle can be seen, but the minimum C_m is almost unchanged. The pulsed blown data shows no moment collapse and no clockwise C_m loop.

Pressure distributions are shown in figure 5. The leading edge is at the top of each frame, and time runs from right to left, with the data plotted starting from the mean angle on the upstroke. The unactuated case, frame (a), shows the dynamic stall as the collapse of leading edge suction just before $\alpha = 24°$ and appearance of enhanced suction around the trailing edge shortly after. The suction pulse during the early part of the downstroke is the result of the stall vortex crossing the trailing edge and subsequent vortex shedding. The steady blowing actuated case, frame (b), shows the dynamic stall also, but there is no post-stall pressure pulse. The pulse blown case, frame (c), shows no evidence of a dynamic stall vortex. Contour edges are rough due to the pulsed blowing. Hilbert transform damping $\Xi(t)$ is shown in figure 6 for the baseline, steady and pulsed blowing cases. The unactuated case has strong negative damping over much of the first half of the oscillation cycle, and this correlates with the phasing of the dynamic stall vortex convection and the secondary shedding. Damping becomes positive during the upstroke. Steady blowing does very little to relieve the magnitude of the initial negative damping during the upstroke, although its phase is delayed, but the damping very quickly becomes positive after the dynamic stall vortex has crossed the trailing edge, and there is no evidence of the

effect of any secondary vortex. The pulsed blown case shows no significant negative damping.

IV Conclusions

Wind tunnel tests to assess the effectiveness of steady and pulsed air jet vortex generators to mitigate against the adverse effects of dynamic stall have been conducted. Pulsed AJVGs can produce a more significant improvement compared to steady blowing at a much lower jet momentum coefficient. Steady blowing is less effective at delaying the onset of dynamic stall, such that in an oscillatory airfoil motion test that shows a deep dynamic stall with negative cycle damping, the pulsed blown jet may show no dynamic stall at all during the pitching cycle.

Acknowledgements

The study used data originally collected under the United Kingdom Defence Aerospace Research Partnership but since analysed via independent means.

References

[1] L.W. Carr. Progress in the analysis and prediction of dynamic stall. *Journal of Aircraft*, 25(1):6–17, 1988.

[2] W.J. McCroskey, K.W. McAlister, L.W. Carr, S.L. Pucci, O. Lambert, and R.F. Indergrand. Dynamic stall on advanced airfoil sections. *Journal of the American Helicopter Society*, 26(3):40–50, 1981.

[3] P.G. Wilby. Shockwaves in the rotor world - a personal perspective of 30 years of rotor aerodynamic developments in the uk. *Aeronautical Journal*, 102(1013):113–128, 1998.

[4] M.S. Chandrasekhara, M.C. Wilder, and L.W. Carr. Compressible dynamic stall control: Comparison of two approaches. *Journal of Aircraft*, 38(3):448–453, 2001.

[5] Y.H. Yu, S. Lee, K.W. McAlister, C. Tung, and C.M. Wang. Dynamic stall control for advanced rotorcraft application. *AIAA Journal*, 33(2):289–295, 1995.

[6] K. Nguyen. Active control of helicopter blade stall. *Journal of Aircraft*, 35(1):91–98, 1998.

[7] R.B. Green, E.A. Gillies, and Y. Wang. Trailing-edge flap flow control for dynamic stall. *Aeronautical Journal*, 115(1170):493–503, 2011.

[8] D. Greenblatt and I. Wygnanski. Dynamic stall control by periodic excitation, part 1: Naca 0015 parametric study. *Journal of Aircraft*, 38(3):430–438, 2001.

[9] C. Singh, D.J. Peake, A. Kokkalis, V. Khodagolian, F.N. Coton, and R.A.M. Galbraith. Control of rotorcraft retreating blade stall using air-jet vortex generators. *Journal of Aircraft*, 43(4):1169–1176, 2006.

[10] A.D. Gardner, K. Richter, H. Mai, and D. Neuhaus. Experimental investigation of high-pressure pulsed blowing for dynamic stall control. *CEAS Aeronautical Journal*, 5:185–198, 2014.

[11] D. Weaver, K.W. McAlister, and J. Tso. Control of vr-7 dynamic stall by strong steady blowing. *Journal of Aircraft*, 41(6):1404–1413, 2004.

[12] H.F. Müller-Vahl, C.N. Nayeri, C.O. Paschereit, and D. Greenblatt. Dynamic stall control via adaptive blowing. *Renewable Energy*, 97:47–64, 2016.

[13] J.P. Johnston and M. Nishi. Vortex generator jets - means for flow separation control. *AIAA Journal*, 28(6):989–994, 1990.

[14] F.S. Henry and H.H. Pearcey. Numerical model of boundary layer control using air-jet generated vortices. *AIAA Journal*, 32(12):2415–2424, 1994.

[15] A.A. Prince and V. Khodagolian. Low-speed static stall suppression using steady and pulsed air-jet vortex generators. *AIAA Journal*, 49(3):642–654, 2011.

[16] F.O. Carta. An analysis of the stall flutter instability of helicopter rotor blades. *Journal of the American Helicopter Society*, 12(4):1–18, 1967.

[17] P.O. Bowles, T.C. Corke, D.G. Coleman, F.O. Thomas, and M. Wasikowski. Improved understanding of aerodynamic damping through the hilbert transformation. *AIAA Journal*, 52(11):2384–2394, 2014.

Open access data files for this work: https://doi.org/10.17862/cranfield.rd.5001947

Figures

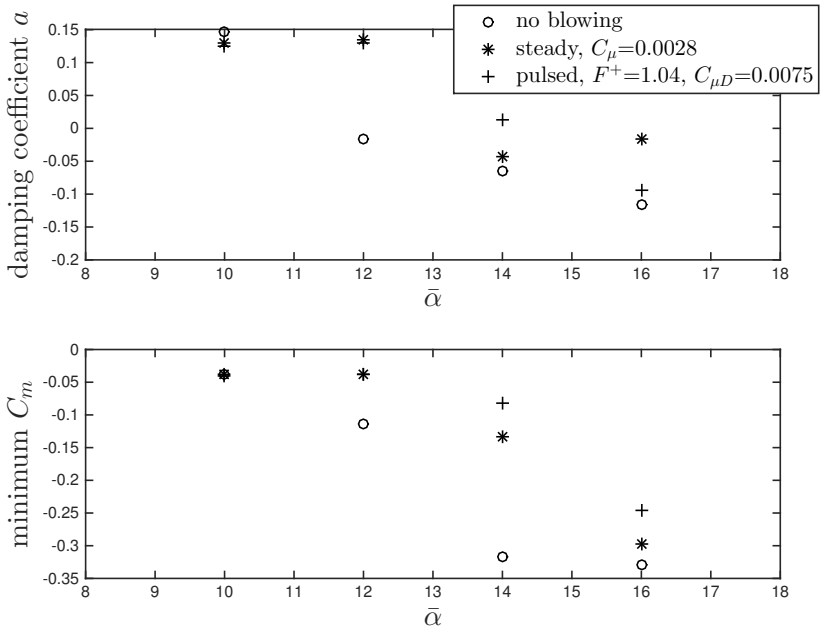

Figure 1: Negative damping thresholds and minimum pitching moment. All tests are at reduced frequency $k = 0.103$, pitch amplitude $\hat{\alpha} = 8^{\circ}$, Reynolds number 1 million. Steady blowing data are at $C_\mu = 0.0028$, pulsed blown data are at $F^+ = 1.04$, duty cycle 0.5, $C_{\mu D} = 0.0075$

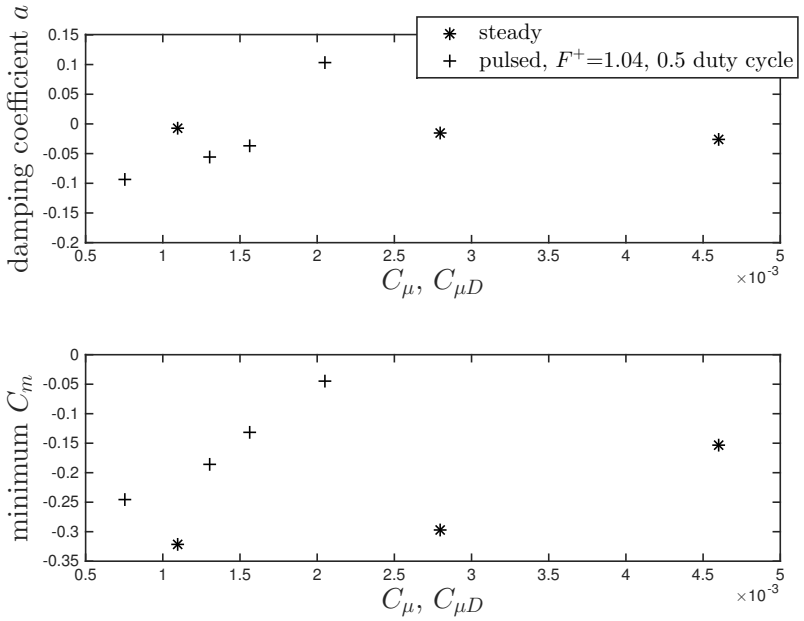

Figure 2: Effect of blowing coefficient for steady and pulsed jet. All tests are at reduced frequency $k = 0.103$, mean angle $\bar{\alpha} = 16^o$, pitch amplitude $\hat{\alpha} = 8^o$, Reynolds number 1 million. Reference case with no blowing has a=-0.116, minimum C_m=-0.328.

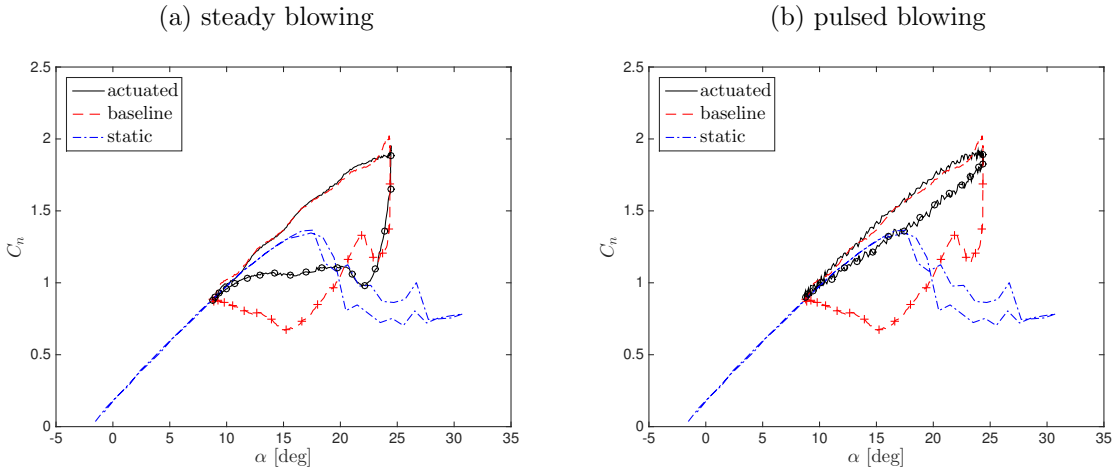

Figure 3: Normal force coefficient C_n cycles for k =0.103, $\hat{\alpha} = 8^o$, $\bar{\alpha} = 16^o$. Frame (a) is for steady blowing at $C_\mu = 0.0028$, frame (b) is for pulsed blowing at $C_\mu = 0.0041$ ($C_{\mu D} = 0.0021$), $F^+ = 1.04$, 0.5 duty cycle. The symbols on the plots indicate the downstroke.

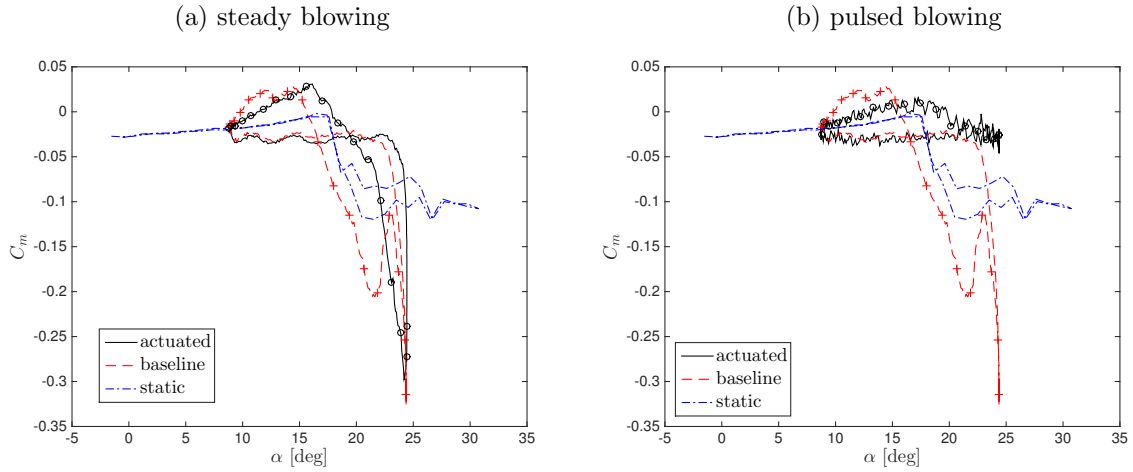

Figure 4: Pitching moment coefficient C_m cycles for k =0.103, $\hat{\alpha} = 8^o$, $\bar{\alpha} = 16^o$. Frame (a) is for steady blowing at $C_\mu = 0.0028$, frame (b) is for pulsed blowing at $C_\mu = 0.0041$ ($C_{\mu D} = 0.0021$), $F^+ = 1.04$, 0.5 duty cycle. The symbols on the plots indicate the downstroke.

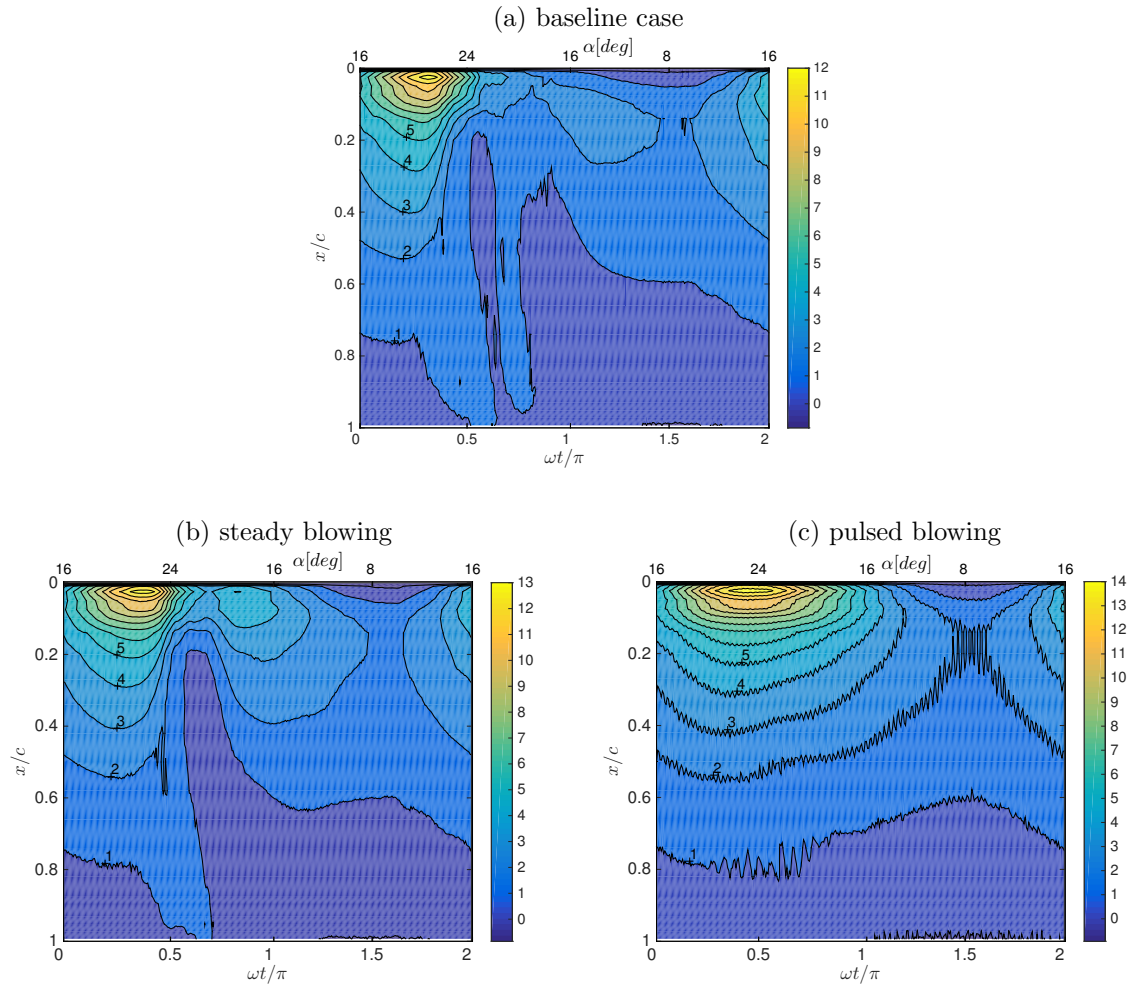

Figure 5: Pressure coefficient C_p cycles for k =0.103, $\hat{\alpha} = 8^o$, $\bar{\alpha} = 16^o$. Frame (a) is the baseline unactuated case, frame (b) is for steady blowing at $C_\mu = 0.0028$, frame (c) is for pulsed blowing at $C_\mu = 0.0041$ ($C_{\mu D} = 0.0021$), $F^+ = 1.04$, 0.5 duty cycle. Contours of $-C_p$ are shown. Contour lines are separated by value of ΔC_p =1, and selected contour levels have been labelled.

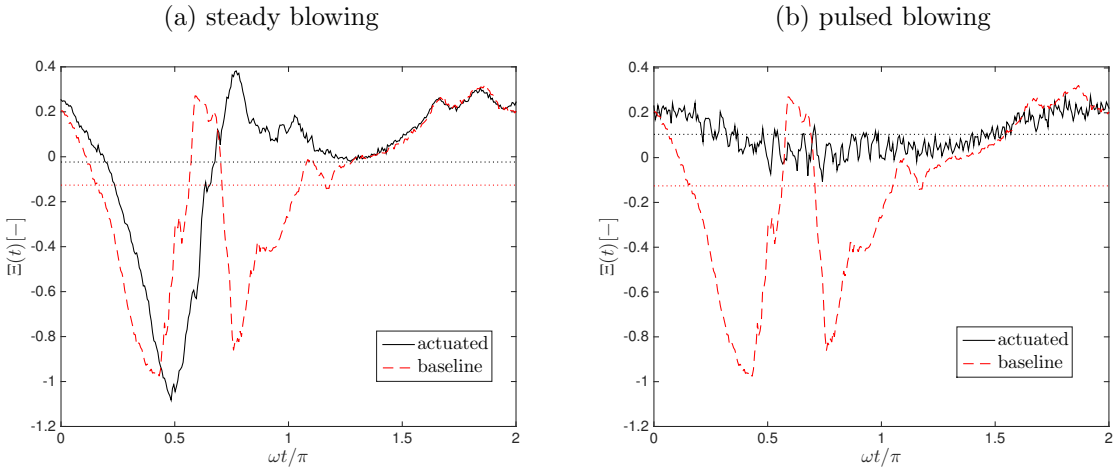

Figure 6: Hilbert transform damping cycle for k =0.103, $\hat{\alpha}$ = 8°, $\bar{\alpha}$ = 16°. Frame (a) is for steady blowing at $C_\mu = 0.0028$, frame (b) is for pulsed blowing at $C_\mu = 0.0041$ ($C_{\mu D} = 0.0021$), $F^+ = 1.04$, 0.5 duty cycle. The horizontal lines are the mean damping over the cycle.